

Behavior-Guided Candidate Calibration for Multimodal Recommendation

Zesheng Li*

University of the Chinese Academy of Sciences
China

2022111515@stu.sufe.edu.cn

Chengchang Pan[†]

University of the Chinese Academy of Sciences
China

166353314@qq.com

Honggang Qi[†]

University of the Chinese Academy of Sciences
China

hgqi@ucas.ac.cn

Abstract

Multimodal recommendation benefits from content signals, but the gain depends on how those signals interact with the ranking pipeline. We find that moderate cross-view agreement helps, while stronger agreement suppresses recommendation-specific variation. Spectral analysis shows a clear split: low-frequency components capture shared structure, and higher-frequency components preserve more discriminative signal. Based on this finding, we introduce a behavior-guided candidate calibration model that converts training-only co-user overlap into signed candidate evidence and applies it only to the shortlist produced by the multimodal backbone. The backbone keeps the representation space stable; behavior evidence acts only where ranking is decided. Results on Amazon Baby, Sports, and Electronics show consistent gains over strong multimodal baselines. Code is available at <https://github.com/LIZESHENG13/bridge>.

CCS Concepts

• **Information systems** → **Recommender systems**; *Multimedia and multimodal retrieval*.

Keywords

Multimodal Recommendation, Dual-Frequency Graph Evidence, Behavior Graph, Candidate Calibration

1 Introduction

Images, titles, descriptions, and brands provide useful side information for recommendation, especially when interaction data are sparse. This has motivated a broad family of multimodal recommenders that combine user-item interactions with visual and textual item features [3, 25–27]. Recent surveys synthesize this literature from representation, modeling, and optimization perspectives [17]. Recent work has improved the representation layer by building item-item graphs from content, denoising multimodal features, or enforcing stronger consistency across views [5, 10, 24, 32, 39]. The common premise is simple: a better multimodal representation should yield a better ranker.

Our diagnostics support a more selective view. Content evidence helps, but only within an effective range. Moderate cross-view consistency improves ranking, whereas stronger consistency suppresses recommendation-specific variation. Frequency analysis further shows a shared-vs-private split: low-frequency bands are aligned across views, while higher-frequency bands retain more

ranking signal. That asymmetry matters because ranking is decided in a narrow candidate set. Once alignment becomes too strong, it blurs the local distinctions that separate plausible items from near neighbors.

BRIDGE turns these observations into a behavior-guided design. The multimodal encoder defines the base candidate geometry, and co-user behavior authorizes only local residual corrections inside that candidate set. DFGE preserves frequency-aware multimodal evidence, BEN converts training-only co-user overlap into signed behavior support, and CRI applies that support only within the candidate scope. On Amazon Baby, Sports, and Electronics, BRIDGE reaches 0.1128, 0.1262, and 0.0778 Recall@20, respectively, with corresponding NDCG@20 values of 0.0525, 0.0594, and 0.0385.

A second gap is operational. In retrieval-and-rank pipelines, the shortlist is already the decision bottleneck. A content signal that helps representation learning can still hurt ranking when it is allowed to move every score in the catalog. BRIDGE isolates that failure mode: the multimodal backbone defines the shortlist, and behavior evidence is allowed to revise only the candidates that the backbone has already made plausible. This localizes correction to the region where ranking is actually decided.

The contributions of this work are:

- We identify two diagnostics in multimodal recommendation: direct cross-view consistency has an effective range, and the representation spectrum separates shared low-frequency evidence from more private higher-frequency variation.
- We propose DFGE, a dual-frequency graph evidence encoder that preserves that spectrum with band routing and structural regularization.
- We propose BEN and CRI, which turn training-only co-user overlap into signed behavior evidence and use it only to calibrate the candidate scope used at training and inference.

2 Related Work

2.1 Multimodal Recommendation and Cross-View Alignment

Multimodal recommendation extends collaborative filtering with visual and textual signals. VBPR [3] shows that content can alleviate sparsity, while graph-based methods such as MMGCN [27], GRCN [26], DualGNN [25], and LATTICE [35] organize these signals with user-item and item-item structure. Recent variants add denoising, diffusion, robustness, dual-path routing, retrieval completion, or stronger cross-view consistency [1, 2, 5, 7–12, 19, 20, 24, 29, 36, 38, 39]. Related alignment and fusion work also explores dual-graph

*First author. Code: <https://github.com/LIZESHENG13/bridge>

[†]Corresponding authors.

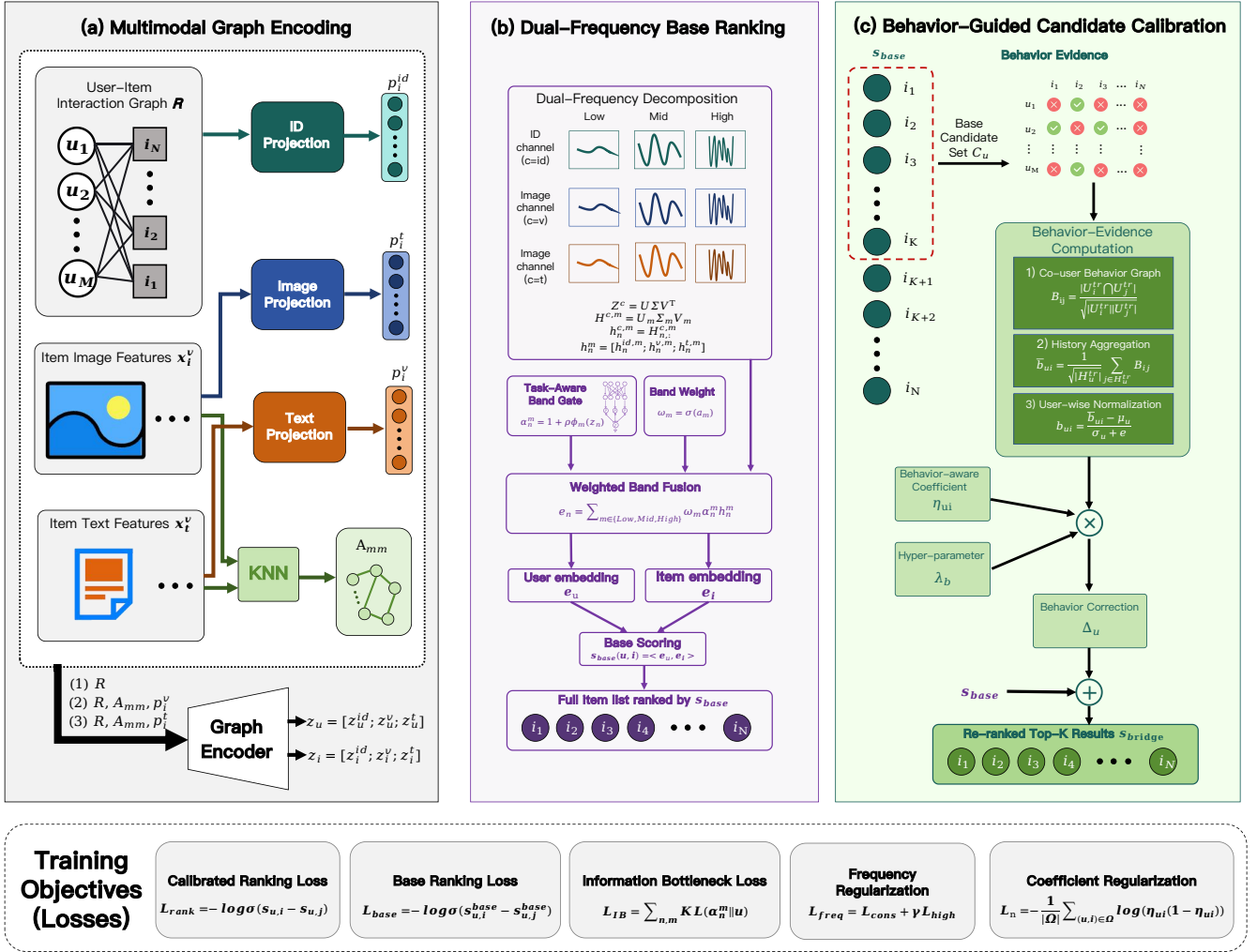


Figure 1: Overview of BRIDGE. DFGE constructs dual-frequency graph evidence; BEN computes normalized behavior support; CRI integrates the residual only inside the selected candidate set.

attention, hierarchical multi-step fusion, and multimodal large language model coupling [21, 23, 31, 34, 40]. The common theme is to improve representation quality before ranking. BRIDGE differs by asking when content evidence should be trusted by the ranker rather than how aggressively it should be fused.

The key distinction is that most alignment methods treat cross-view agreement as a proxy for better ranking. In practice, that assumption is too strong. Once content matching becomes dominant, it can erase the differences that separate a plausible item from a near duplicate or a popular lookalike. BRIDGE keeps the same multimodal evidence, but uses it to define candidate geometry rather than to rewrite every score in the catalog. The question is not whether two views can be aligned. The question is whether that alignment should change the rank of a specific candidate.

This is why the strongest recent alignment systems still leave a gap. They can improve the encoder, the fusion block, or the item graph, but they do not decide when the resulting evidence should

be allowed to alter the shortlist. BRIDGE treats that decision as part of the model, not a post-hoc choice.

2.2 Frequency-Aware and Behavior-Guided Recommendation

Frequency-aware recommenders separate stable structure from fine-grained variation. SMORE [16], FITMM [32], SSR [33], MSCFNet [6], DuGRec [13], D-DPDG [28], and Sequences-as-Nodes [23] show that spectral views can organize multimodal or collaborative evidence. These works differ in whether the spectrum is used for denoising, co-frequency enhancement, or explicit band routing. BRIDGE uses the same general intuition but keeps the band decomposition as a representation core rather than a standalone predictor.

That makes BRIDGE different from frequency-aware denoising pipelines. Those models usually use the spectrum to suppress noise or separate stable from unstable components, while BRIDGE uses

the decomposition to decide which bands remain shared evidence and which bands are left as residual variation for candidate calibration. The band split is therefore an authorization step, not only a regularizer.

The same point applies to band routing. A decomposition can denoise a representation, but denoising alone does not explain how the output should affect ranking. BRIDGE keeps the spectrum inside the backbone and lets candidate calibration consume only the bands that remain useful after decomposition. This keeps the representation and the calibration rule aligned with one another.

2.3 Behavior-Guided, Causal, and Sequential Multimodal Control

In parallel, behavior-guided methods such as BPR [22], LightGCN [4], DRAGON [37], FGCM [15], JBM-Diff [18], and causal-inspired multimodal recommendation [30] use interaction structure to validate or filter content-derived relations. More recent work extends this idea to dual-graph diffusion, modality coherence, and multi-intention or sequential settings [2, 12, 21, 31, 34, 41]. BRIDGE combines these lines, but uses behavior only as a local authorization signal for candidate-level residual calibration rather than as a global fusion or denoising target.

That distinction matters because many behavior-guided methods still operate globally. They improve the score function, the graph structure, or the fusion rule, but the behavior signal is applied across the item space. BRIDGE keeps the same evidence and narrows its effect to a top- K candidate set, which makes the behavior branch easier to interpret and less likely to distort the catalog-wide ranking order.

Together, these strands motivate BRIDGE’s dual-frequency and candidate-calibrated design.

3 Problem Formulation

Let \mathcal{U} and \mathcal{I} denote the user and item sets. We observe implicit feedback $\mathcal{R} = \{(u, i) \mid u \in \mathcal{U}, i \in \mathcal{I}\}$, where an edge indicates that user u interacted with item i . Each item also has multimodal content features, including visual features \mathbf{x}_i^v and textual features \mathbf{x}_i^t . For a user u , let \mathcal{H}_u be the interacted item set; for an item i , let \mathcal{U}_i be the set of users who interacted with it. The recommendation task is to learn a score $s(u, i)$ and rank unobserved items for each user under full-sort evaluation.

The standard training objective is pairwise Bayesian Personalized Ranking (BPR) [22]:

$$\mathcal{L}_{\text{BPR}}(s) = - \sum_{(u,i,j)} \log \sigma(s(u, i) - s(u, j)), \quad (1)$$

where i is an observed positive item and j is a sampled negative item. Existing multimodal recommenders usually define $s(u, i)$ by making collaborative, visual, and textual embeddings consistent or fusing them. In this work, we make the scoring problem more explicit: content-derived signals are allowed to affect ranking only when supported by behavior evidence.

BRIDGE learns a final score of the form

$$s(u, i) = s_{\text{base}}(u, i) + \Delta_{\text{bridge}}(u, i), \quad (2)$$

where the residual correction is behavior-guided and applied only in a controlled candidate scope. The concrete definitions of behavior evidence and the frequency-aware encoder are given in Method.

4 Motivating Observations

BRIDGE is motivated by three empirical observations. Together they suggest a simple design principle: multimodal information should be preserved, but content should be treated as conditional evidence, not as a command.

4.1 Direct Consistency Has an Effective Range

We run a compact direct-consistency diagnostic on Amazon Baby using the same backbone and split, while varying only the consistency strength. Without direct consistency, Recall@20 is 0.0922. A moderate setting with a contrastive loss weight of 0.01, a similarity weight of 0.3, and UI cosine improves it to 0.1024, showing that cross-view consistency can be useful. However, a stronger setting with a contrastive loss weight of 0.1 and a similarity weight of 1.0 drops Recall@20 to 0.0836, showing that direct consistency has an effective range. Once this objective dominates, it can suppress private recommendation factors that are not shared by all modalities. We also checked a lighter setting with a contrastive loss weight of 0.001 and a similarity weight of 0.1 under another seed, which reached Recall@20 of 0.0982 and still stayed below the moderate setting.

4.2 Low Frequency Agrees; High Frequency Ranks

Frequency diagnostics further clarify where the useful information lives. Low-frequency components show strong cross-view agreement, while high-frequency components show weaker agreement. Recommendation performance follows the opposite pattern: high-frequency views rank better than low-frequency views, although both are weaker than the complete representation. Figure 2 visualizes this diagnostic as a pair of range plots. The bands here are representation-spectral bands obtained from graph-smoothed channel matrices, not graph Laplacian eigenvectors; Section 5.1 gives the formal interpretation. This motivates a useful split: low frequency is a natural substrate for shared structure, whereas higher-frequency variation carries more local ranking evidence that should be handled cautiously.

4.3 Behavior Evidence Decides When Calibration Helps

Content-derived corrections are not uniformly beneficial. In our diagnostics, global score correction often hurts, while top- K candidate correction can improve ranking. Co-user behavior evidence is also consistently strong, especially on sparse Amazon domains. We therefore interpret behavior evidence as a local validity test for candidate calibration. If a candidate is also supported by user co-occurrence, a small correction may recover items missed by sparse collaborative training. If not, the same content relation may simply identify substitutes or visual lookalikes.

These observations lead to three design requirements for BRIDGE:

Table 1: Overall recommendation performance on three Amazon datasets. All methods use the same processed splits, BEIT3 features, and full-sort evaluation protocol. BRIDGE is selected by best validation Recall@20 under the same setting. Results of the strongest baselines and our method are reported with mean \pm standard deviation over 5 random seeds. ** denotes statistical significance at $p < 0.01$ under independent two-sample t -test against the best baseline.

Dataset	Metric	BPR	LightGCN	VBPR	MMGCN	GRCN	DualGNN	SLMRec	LATTICE	BM3	FREEDOM	DiffMM	MMIL	AlignRec	SMORE	FITMM	BRIDGE
Baby	R@10	0.0357	0.0479	0.0418	0.0413	0.0538	0.0507	0.0533	0.0561	0.0573	0.0624	0.0617	0.0670	0.0674 \pm 0.0007	0.0680 \pm 0.0008	0.0716 \pm 0.0006	0.0759 ** \pm 0.0004
	R@20	0.0575	0.0754	0.0667	0.0649	0.0832	0.0782	0.0788	0.0867	0.0904	0.0985	0.0978	0.1035	0.1046 \pm 0.0010	0.1035 \pm 0.0011	0.1089 \pm 0.0009	0.1128 ** \pm 0.0006
	N@10	0.0192	0.0257	0.0223	0.0211	0.0285	0.0264	0.0291	0.0305	0.0311	0.0324	0.0321	0.0361	0.0363 \pm 0.0004	0.0365 \pm 0.0005	0.0387 \pm 0.0005	0.0428 ** \pm 0.0003
	N@20	0.0249	0.0328	0.0287	0.0275	0.0364	0.0335	0.0365	0.0383	0.0395	0.0416	0.0408	0.0455	0.0458 \pm 0.0005	0.0457 \pm 0.0006	0.0484 \pm 0.0005	0.0525 ** \pm 0.0003
Sports	R@10	0.0432	0.0569	0.0561	0.0394	0.0607	0.0574	0.0667	0.0628	0.0659	0.0705	0.0687	0.0747	0.0758 \pm 0.0008	0.0762 \pm 0.0009	0.0809 \pm 0.0007	0.0860 ** \pm 0.0004
	R@20	0.0653	0.0864	0.0857	0.0625	0.0928	0.0881	0.0998	0.0961	0.0987	0.1077	0.1035	0.1133	0.1160 \pm 0.0012	0.1142 \pm 0.0013	0.1187 \pm 0.0010	0.1262 ** \pm 0.0007
	N@10	0.0241	0.0311	0.0305	0.0203	0.0335	0.0316	0.0366	0.0339	0.0357	0.0382	0.0357	0.0405	0.0414 \pm 0.0005	0.0408 \pm 0.0005	0.0441 \pm 0.0004	0.0490 ** \pm 0.0002
	N@20	0.0298	0.0387	0.0386	0.0266	0.0421	0.0393	0.0454	0.0431	0.0443	0.0478	0.0458	0.0505	0.0517 \pm 0.0006	0.0506 \pm 0.0006	0.0538 \pm 0.0005	0.0594 ** \pm 0.0004
Electronics	R@10	0.0235	0.0363	0.0293	0.0207	0.0349	0.0363	0.0392	0.0397	0.0437	0.0382	0.0418	0.0456	0.0472 \pm 0.0008	0.0474 \pm 0.0009	0.0503 \pm 0.0006	0.0549 ** \pm 0.0002
	R@20	0.0367	0.0540	0.0458	0.0331	0.0529	0.0541	0.0581	0.0573	0.0648	0.0588	0.0617	0.0673	0.0700 \pm 0.0010	0.0691 \pm 0.0012	0.0725 \pm 0.0009	0.0778 ** \pm 0.0004
	N@10	0.0127	0.0204	0.0159	0.0109	0.0195	0.0202	0.0223	0.0224	0.0247	0.0209	0.0224	0.0253	0.0262 \pm 0.0004	0.0261 \pm 0.0004	0.0278 \pm 0.0003	0.0326 ** \pm 0.0002
	N@20	0.0161	0.0250	0.0202	0.0141	0.0241	0.0248	0.0273	0.0271	0.0302	0.0262	0.0278	0.0309	0.0321 \pm 0.0005	0.0318 \pm 0.0005	0.0335 \pm 0.0004	0.0385 ** \pm 0.0003

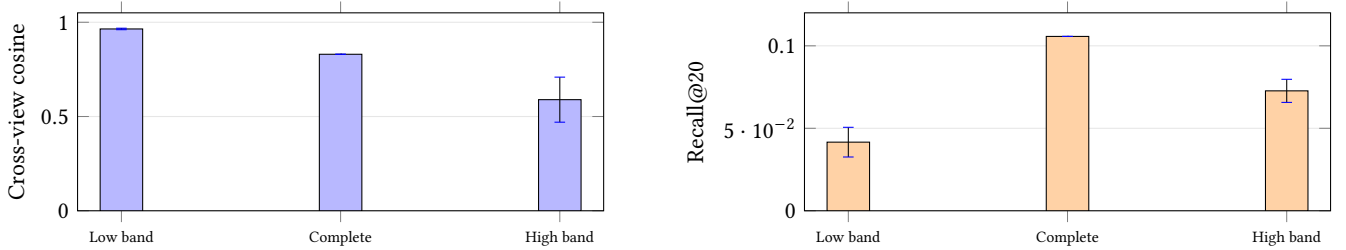


Figure 2: Representation-spectral frequency diagnostic on Amazon Baby. Error bars denote the observed ranges. Leading singular-energy bands are more cross-view consistent, while later bands retain stronger ranking signal than the leading bands but remain insufficient as a standalone ranker. This is an SVD ordering in the learned latent space, not a Laplacian eigenmode plot.

- (1) Preserve frequency-aware multimodal structure instead of collapsing all signals into an undifferentiated representation.
- (2) Use behavior evidence inside the model so that user histories can authorize or reject candidate corrections.
- (3) Restrict score calibration to the candidate set, so uncertain evidence cannot perturb the whole item space.

5 Method

Figure 1 summarizes BRIDGE. The method follows one principle: frequency-specific multimodal evidence should be preserved before behavior evidence calibrates the final ranking. BRIDGE separates this process into three modules. DFG learns the frequency-aware graph representation and base score $s_{\text{base}}(u, i)$. BEN estimates normalized behavior evidence b_{ui} from the training interaction graph. CRI injects that evidence as a signed residual only inside the candidate scope. The base encoder therefore defines the ranking geometry, and the behavior branch only adjusts local decisions.

5.1 Dual-Frequency Graph Evidence Encoder

Each item has an ID embedding, a visual feature, and a textual feature. The visual and textual features are projected to the same latent dimension as the ID channel. DFG first applies channel-specific projection, then two rounds of symmetric normalized message passing on the user-item graph, and finally sums the layer states

to form each channel embedding. Let A_{ui} denote the user-item adjacency and $\hat{A}_{ui} = D^{-\frac{1}{2}} A_{ui} D^{-\frac{1}{2}}$ its symmetric normalization. For channel c , the input state is $H^{c,(0)} = [P_u^c; W_c x_i^c]$, where P_u^c is a learned user preference table and W_c is a linear projection for that channel; for the ID channel, the second term is the learned item ID embedding. We then apply $L = 2$ rounds of normalized message passing, $H^{c,(t+1)} = \hat{A}_{ui} H^{c,(t)}$, and read out the channel embedding by summing all layers, $Z^c = \sum_{t=0}^L H^{c,(t)}$, for $c \in \{\text{id}, v, t\}$. The item-side representation is refined with a cached multimodal item graph built from top- K cosine neighbors over the content features. When both image and text are available, the cached item graph is the weighted sum $0.1 A_v + 0.9 A_t$ with $K = 10$. The item graph acts as a second smoothing stage before frequency decomposition, using one propagation stage and keeping the final smoothed item states rather than another layer-sum readout. This produces user and item representations for the ID, visual, and textual channels:

$$z_u^c, z_i^c = \text{GraphEnc}_c(\mathcal{R}, A_{\text{mm}}, x^c), \quad c \in \{\text{id}, v, t\}. \quad (3)$$

The three channels are then concatenated:

$$z_u = [z_u^{\text{id}}; z_u^v; z_u^t], \quad z_i = [z_i^{\text{id}}; z_i^v; z_i^t]. \quad (4)$$

Each channel has dimension 64, so the fused representation dimension is 192.

5.2 Spectral Band Routing

DFGE decomposes each modality channel into M frequency bands before producing the base ranking embedding. For a representation matrix \mathbf{Z}^c of modality c , we compute a singular decomposition $\mathbf{Z}^c = \mathbf{U}\Sigma\mathbf{V}^\top$ and split the singular components into M contiguous bands. The m -th band is:

$$\mathbf{H}^{c,m} = \mathbf{U}_m \Sigma_m \mathbf{V}_m^\top. \quad (5)$$

For each node n and channel c , let $\mathbf{h}_n^{c,m} = (\mathbf{H}^{c,m})_{n,\cdot}$, denote the m -th band slice. The band-specific multimodal state is then

$$\mathbf{h}_n^m = [\mathbf{h}_n^{\text{id},m}, \mathbf{h}_n^{v,m}, \mathbf{h}_n^{t,m}], \quad n \in \mathcal{U} \cup \mathcal{I}. \quad (6)$$

A task-aware band gate then fuses the bands:

$$\alpha_n^m = 1 + \rho \cdot \phi_m(\mathbf{z}_n), \quad \omega_m = \sigma(a_m), \quad (7)$$

$$\mathbf{e}_n = \sum_{m=1}^M \omega_m \alpha_n^m \mathbf{h}_n^m. \quad (8)$$

Here $\phi(\mathbf{z}_n) = \sigma(\mathbf{W}_g \mathbf{z}_n + \mathbf{b}_g)$ is a one-layer gate network with output dimension M ; in the main setting, $\phi_m(\cdot)$ is the m -th sigmoid output of this linear gate, and ρ is a learned scalar initialized to 0.5. The base score is computed by inner product:

$$s_{\text{base}}(u, i) = \langle \mathbf{e}_u, \mathbf{e}_i \rangle. \quad (9)$$

The frequency decomposition is part of the base ranking representation. Low-frequency bands, in the sense of leading singular directions of the propagated representation spectrum, provide shared graph evidence, whereas higher-frequency bands preserve private ranking variation. CRI later decides whether the resulting candidate score should receive a behavior-authorized residual; BRIDGE does not add a separate high-frequency score to every item.

Interpretation of frequency. Here, frequency refers to a representation-spectral ordering rather than a Laplacian eigenbasis. Let $\mathbf{Z} \in \mathbb{R}^{N \times d}$ be a graph-smoothed channel matrix after message passing. BRIDGE computes $\mathbf{Z} = \mathbf{U}\Sigma\mathbf{V}^\top$, partitions the right singular directions as $\mathbf{V} = [\mathbf{V}_1, \dots, \mathbf{V}_M]$ in descending singular-value order, and reconstructs band evidence by $\mathbf{H}^m = \mathbf{Z}\mathbf{V}_m\mathbf{V}_m^\top$. The leading bands capture dominant post-smoothing variation, while later bands collect residual directions with less shared energy. Because normalized graph propagation is already low-pass, the leading singular bands act as stable shared evidence and the trailing bands retain more local variation. A graph Laplacian basis would order components by graph oscillation rather than latent energy; BRIDGE therefore states its frequency claims for this representation-spectral decomposition.

Channel-wise decomposition. The decomposition is applied at the modality-channel level rather than on the concatenated matrix. Each user/item representation is split into 64-dimensional ID, image, and text blocks; each block is decomposed separately and then reassembled into 192-dimensional band representations. With $M = 3$, the 64 singular directions are partitioned into bands of size 22/21/21 in descending singular-value order. For controlled analysis, we also evaluate non-SVD decomposition operators under the same encoder and fusion capacity. In the equal-capacity no-decomposition control, the band inputs are

$$\mathbf{H}^{c,m} = \frac{1}{M} \mathbf{Z}^c, \quad m = 1, \dots, M. \quad (10)$$

This keeps the same number of band gates, band weights, graph encoders, and fusion parameters while removing spectral separation itself. We also evaluate fixed-basis variants in which $\mathbf{H}^{c,m} = \mathbf{Z}^c \mathbf{Q}_m \mathbf{Q}_m^\top$: Gram uses eigenvectors of $\mathbf{Z}^\top \mathbf{Z}$, DCT uses a deterministic cosine basis, and Random uses a fixed orthogonal basis.

5.3 Behavior Evidence Normalizer

The Behavior Evidence Normalizer (BEN) builds an item-item behavior graph from co-user similarity after the interaction split is fixed. Let \mathcal{D}_{tr} denote the training interactions only, and let $\mathcal{U}_i^{\text{tr}}$ denote the users who interacted with item i in \mathcal{D}_{tr} . The raw behavior edge between two items is:

$$B_{ij} = \frac{|\mathcal{U}_i^{\text{tr}} \cap \mathcal{U}_j^{\text{tr}}|}{\sqrt{|\mathcal{U}_i^{\text{tr}}|} \sqrt{|\mathcal{U}_j^{\text{tr}}|}}. \quad (11)$$

Only the top K_b neighbors of each item are kept. For a user-item pair (u, i) , the raw candidate behavior evidence is aggregated from the user's training history $\mathcal{H}_u^{\text{tr}}$:

$$\tilde{b}_{ui} = \frac{1}{\sqrt{|\mathcal{H}_u^{\text{tr}}|}} \sum_{j \in \mathcal{H}_u^{\text{tr}}} B_{ij}. \quad (12)$$

Validation and test interactions are never used to construct B_{ij} , $\mathcal{H}_u^{\text{tr}}$, item popularity, or user degree features; they are used only for model selection and final evaluation. The reported setting uses cosine co-user similarity, $K_b = 1000$, square-root history normalization, and centered behavior scores:

$$b_{ui} = \frac{\tilde{b}_{ui} - \mu_u}{\sigma_u + \epsilon}. \quad (13)$$

Although B_{ij} and \tilde{b}_{ui} are non-negative, the normalized residual b_{ui} can be positive or negative. Positive values indicate stronger-than-usual behavior support under the user's history, while negative values indicate weaker-than-usual support and can demote a candidate when used in Eq. 20. When the full user-item behavior matrix fits in memory, BRIDGE normalizes each user's complete behavior row once and reuses the same b_{ui} values in sampled training pairs and candidate inference. For larger sparse datasets, b_{ui} is computed on demand; both paths yield the same normalized score and avoid hidden train-test mismatch.

5.4 Candidate Residual Integrator

The Candidate Residual Integrator (CRI) uses BEN evidence as a signed score residual after DFGE has selected a candidate set. The central design choice is the candidate-level scope rather than an unconstrained learned coefficient. The main BRIDGE setting uses a validation-selected residual strength:

$$\Delta_{\text{bridge}}(u, i) = \mathbb{I}[i \in \mathcal{C}_u^{\text{tr}}] \lambda_b b_{ui}. \quad (14)$$

This is the formulation used in the main experiments. We also include a conservative control with lightweight user and item biases β_u, β_i and scalar coefficients a_s, a_b :

$$\eta_{ui} = \sigma(\beta_u + \beta_i + a_s \tanh(s_{\text{base}}(u, i)) + a_b \tanh(b_{ui})). \quad (15)$$

The corresponding candidate score is

$$s_{\text{train}}(u, i) = s_{\text{base}}(u, i) + \mathbb{I}[i \in \mathcal{C}_u^{\text{tr}}] \lambda_b \eta_{ui} b_{ui}. \quad (16)$$

In both cases, the sign of the correction comes from b_{ui} ; the coefficient only scales the residual. This distinction matters empirically: the fixed- λ_b calibrator is the primary CRI instantiation, while the conservative coefficient remains a useful control. During training, BRIDGE uses the same candidate scope as inference. For each training user, we first form a detached base-score candidate set:

$$C_u^{\text{tr}} = \text{TopK}(\text{sg}(s_{\text{base}}(u, \cdot)), K_c), \quad (17)$$

where $\text{sg}(\cdot)$ denotes stop-gradient. This set is computed with the same candidate size K_c used at inference. It is used only as a scope mask, not as an additional supervision target. In the reported setting, the set is recomputed for each mini-batch from detached base embeddings rather than cached across epochs, so the candidate scope tracks the evolving base scorer. Sampled positive and negative items are then scored as:

$$s_{\text{train}}(u, i) = s_{\text{base}}(u, i) + \mathbb{I}[i \in C_u^{\text{tr}}] \lambda_b b_{ui}. \quad (18)$$

The indicator ensures that the residual branch is active only on candidate items. Items outside C_u^{tr} still contribute through $s_{\text{base}}(u, i)$, so the base scorer can learn to move future positives into the candidate set. Gradients are taken through the base score for all sampled pairs and through the calibration coefficient only when the conservative control is used; the top- K membership itself is detached. This candidate-aware objective reduces the train-test scope mismatch of training a residual on globally sampled pairs while applying it only to a top- K candidate set at inference. During inference, BRIDGE first obtains a candidate set from the base multimodal score:

$$C_u = \text{TopK}(s_{\text{base}}(u, \cdot), K_c). \quad (19)$$

At inference, the final score is:

$$s(u, i) = s_{\text{base}}(u, i) + \mathbb{I}[i \in C_u] \lambda_b b_{ui}. \quad (20)$$

This top- K restriction is the main operational scope. It lets behavior evidence reorder plausible candidates, but prevents it from rewriting the whole item space. The reported setting uses $K_c = 200$, and λ_b is selected on validation Recall@20 from a small calibration grid. The conservative coefficient shares the same score form and candidate scope, but it is used only in the control variant. BRIDGE therefore always performs behavior-residual candidate calibration, and the calibration strength is selected on validation rather than tuned on test.

Candidate-aware training. A simpler implementation would train Eq. 18 without the indicator and then apply Eq. 20 only inside C_u at test time. We treat that variant as a reranking baseline and compare against it in the control suite. BRIDGE instead trains the residual under the same scope used at inference, which keeps the residual branch focused on candidate items and leaves the base scorer responsible for moving new positives into the candidate set.

5.5 Training Objective

BRIDGE optimizes the calibrated BPR loss:

$$\mathcal{L}_{\text{rank}} = - \sum_{(u,i,j)} \log \sigma(s_{\text{train}}(u, i) - s_{\text{train}}(u, j)). \quad (21)$$

An auxiliary BPR loss on the base score keeps the backbone predictive:

$$\mathcal{L}_{\text{base}} = - \sum_{(u,i,j)} \log \sigma(s_{\text{base}}(u, i) - s_{\text{base}}(u, j)). \quad (22)$$

This auxiliary loss matters under candidate-aware training: when a positive item is not yet in C_u^{tr} , the residual branch is inactive, and the base loss supplies the learning signal that can move the item into later candidate sets. The frequency gates are regularized by two objectives: an information-bottleneck surrogate that controls gate expansion, and a frequency structural regularizer that constrains the decomposed bands. Let $\gamma_{n,m}$ denote the frequency gate value for node n and band m , and define $\delta_{n,m} = \max(\gamma_{n,m} - 1, 0)$ under the positive-gate setting. The information-bottleneck surrogate is:

$$\mathcal{L}_{\text{IB}} = \frac{1}{|\mathcal{N}|} \sum_{n \in \mathcal{N}} \left[\alpha_{\text{IB}} \|\delta_n\|_2^2 + \mu_{\text{IB}} \|\delta_n\|_2 \sum_{m=1}^M \max(\delta_{n,m} - \phi_+, 0) \right], \quad (23)$$

where \mathcal{N} includes the user and item nodes used by the encoder. This term penalizes unnecessary expansion of the frequency gates: if a node can be represented without strongly amplifying a particular frequency band, the gate is encouraged to stay close to one.

For a training mini-batch $\mathcal{B} = \{(u_b, i_b, j_b)\}_{b=1}^B$, BRIDGE computes the frequency structural regularizer from the user bands $\mathbf{h}_{u_b}^m$ and the positive-item bands $\mathbf{h}_{i_b}^m$. Let $\tilde{\mathbf{h}} = \mathbf{h}/(\|\mathbf{h}\|_2 + \epsilon)$ denote the normalized band vector. The regularizer has two parts:

$$\mathcal{L}_{\text{freq}} = \mathcal{L}_{\text{dec}} + \mathcal{L}_{\text{disc}}, \quad (24)$$

where

$$\mathcal{L}_{\text{dec}} = \frac{1}{BM(M-1)} \sum_{b=1}^B \sum_{m \neq \ell} \left[\cos^2(\tilde{\mathbf{h}}_{u_b}^m, \tilde{\mathbf{h}}_{u_b}^\ell) + \cos^2(\tilde{\mathbf{h}}_{i_b}^m, \tilde{\mathbf{h}}_{i_b}^\ell) \right], \quad (25)$$

and

$$\mathcal{L}_{\text{disc}} = - \frac{1}{B|\mathcal{M}_h|} \sum_{m \in \mathcal{M}_h} \sum_{b=1}^B \log \frac{\exp(\langle \tilde{\mathbf{h}}_{u_b}^m, \tilde{\mathbf{h}}_{i_b}^m \rangle / \tau)}{\sum_{r=1}^B \exp(\langle \tilde{\mathbf{h}}_{u_b}^m, \tilde{\mathbf{h}}_{i_r}^m \rangle / \tau)}. \quad (26)$$

Here \mathcal{M}_h denotes the higher-frequency bands. The decorrelation term suppresses redundant overlap between different bands, while the high-frequency discrimination term keeps the higher-frequency bands ranking-aware by contrasting each positive pair against other positive items in the same batch. This regularizer is structural rather than a strict orthogonality penalty: it preserves a stable band geometry while keeping the informative bands discriminative. In other words, the IB surrogate controls how much each node may amplify frequency bands, whereas the frequency structural regularizer controls the geometry of the resulting band embeddings. When the conservative coefficient control is enabled, we add a soft constraint on the average gate value:

$$\mathcal{L}_\eta = (\mathbb{E}_{(u,i)} [\eta_{ui}] - \tau_\eta)^2. \quad (27)$$

For the main fixed- λ_b BRIDGE setting, $\mathcal{L}_\eta = 0$. The final objective is:

$$\mathcal{L} = \mathcal{L}_{\text{rank}} + \lambda_{\text{base}} \mathcal{L}_{\text{base}} + \lambda_{\text{IB}} \mathcal{L}_{\text{IB}} + \lambda_{\text{freq}} \mathcal{L}_{\text{freq}} + \lambda_\eta \mathcal{L}_\eta. \quad (28)$$

In the reported fixed- λ_b setting, the active coefficients are $\lambda_{\text{base}} = 0.2$, $\lambda_{\text{IB}} = 1.0$, $\lambda_{\text{freq}} = 0.001$, and $\lambda_\eta = 0$. The conservative coefficient control uses $\lambda_\eta = 0.001$ and gate target $\tau_\eta = 0.5$. The candidate-calibration strength follows the same five-point validation grid. This objective makes the method explicit: DFGE learns

the frequency-organized multimodal representation, and CRI integrates BEN evidence under the same candidate scope used by inference.

6 Experiments

6.1 Experimental Setup

We evaluate BRIDGE on Amazon Baby, Sports, and Electronics from the Amazon review benchmark [14] under the common MMRec-style implicit-feedback split. Baby has 19,445 users, 7,050 items, and 160,792 interactions. Sports has 35,598 users, 18,357 items, and 296,337 interactions. Electronics has 192,403 users, 63,001 items, and 1,689,188 interactions. We use BEIT3-derived multimodal features and report Recall@10, Recall@20, NDCG@10, and NDCG@20. For fair comparison, all baselines in Table 1 are evaluated under the same processed interaction splits, the same BEIT3 feature files, and the same full-sort evaluation protocol. The strongest baselines are therefore compared in our setting rather than under a different feature or split configuration. Unless otherwise stated, reported numbers use seed 2020.

For all three datasets, the behavior graph is constructed strictly from the training split. Each interaction file carries a training, validation, or test partition marker. We first build \mathcal{D}_t from the training partition and compute co-user edges, user histories, item popularity, and user degree from this training matrix only. Validation and test interactions are not used in the behavior graph. Baby contains 118,551 training interactions, 20,559 validation interactions, and 21,682 test interactions. Sports contains 218,409 training interactions, 37,899 validation interactions, and 40,029 test interactions. Electronics contains 1,254,441 training interactions, 211,296 validation interactions, and 223,451 test interactions. No cold-start users are present in validation or test after filtering, so the same leakage-free construction is used on all three datasets.

All BRIDGE main results use candidate-aware training. For each training mini-batch, the model computes the detached base top- K_c candidate set of each involved user and masks the behavior residual outside this set, as defined in Eq. 18. At test time, the same K_c -restricted residual is applied to the base top- K_c list in Eq. 20. Thus the residual branch is trained and evaluated under the same candidate-level scope. The training sampler is still pairwise BPR rather than a full listwise reranker, but it avoids the stronger mismatch in which a residual is learned globally and used only locally.

The reported hyperparameters follow the dataset and model configuration files. We use a 64-dimensional embedding size, two graph layers, and three frequency bands. The item graph uses 10 neighbors. The learning rate is 10^{-4} , the regularization weight is 10^{-3} , the IB weight is 1.0, the behavior top- K is 1000, the behavior weight is 0.4, the behavior evaluation top- K is 200, and the train candidate top- K is 200. The behavior graph uses cosine similarity, sum-sqrt aggregation, and z-score normalization. Training uses Adam for 300 epochs with batch sizes 2048 and 4096, zero weight decay, and seed 2020. These settings are shared by the main tables, the ablation suite, and the calibration sweeps. The experiment suite is organized to match the method: Table 1 compares overall ranking quality, Tables 2 and 3 isolate the residual and spectral controls,

and Table 4 checks whether the gains come from a head-item boost or from a broader redistribution of ranking mass.

6.2 Main Results

Table 1 follows the common overall comparison format and places BRIDGE in the rightmost column. The baseline set spans pairwise ranking (BPR [22]) and graph collaborative models (LightGCN [4], MMGCN [27], GRCN [26], DualGNN [25], and LATTICE [35]). It also includes multimodal variants (VBPR [3], SLMRec [24], BM3 [39], FREEDOM [38], DiffMM [5], MMIL [31], AlignRec [10], SMORE [16], and FITMM [32]). The comparison therefore covers classical collaborative ranking and recent multimodal systems under the same data pipeline. We select the checkpoint and candidate-calibration setting by validation Recall@20. The validation grid sets λ_b to 0.1, 0.2, 0.4, 0.6, or 0.8, and also evaluates a coefficient-controlled variant. The test set is evaluated only after this selection. On the three reported datasets, the selected BRIDGE setting is the fixed- λ_b candidate calibration rather than the conservative coefficient control. For the recent strong baselines and BRIDGE, we report mean and standard deviation across five seeds because these methods define the competitive margin. The remaining baselines are included as single-run protocol controls under the same processed data and feature setting. Hyperparameters are chosen on validation Recall@20 using the ranges provided by the corresponding implementations or MMRec-style configuration files. Table 1 shows that BRIDGE improves every metric on every dataset. The Recall gains are consistent, but the NDCG gains are larger, which means the method mainly sharpens the order near the top of the list rather than only recovering more positives at larger cutoffs. The margin is most pronounced on Electronics, where sparsity and popularity skew make a global residual less reliable. This matches the design of BRIDGE: DFGE sets the candidate geometry, and BEN/CRI refines only the items that already look plausible under the multimodal backbone. Broken down by dataset, Baby shows the smallest but still stable gain, Sports shows the largest balanced improvement across Recall and NDCG, and Electronics shows the clearest benefit from candidate-level calibration. This pattern is consistent with the data regime: as the interaction graph becomes sparser, the model benefits more from a restricted residual than from a global score adjustment.

6.3 Diagnostics

At the validation-selected Baby checkpoint, the pair coefficient mean is 0.7365, the behavior correction absolute mean is 0.6886, the low-item norm mean is 6.3819, the high-item norm mean is 2.7333, and the low-high item cosine is 0.0560. These values are consistent with the view that the two frequency components capture different signals and that the residual branch acts as a local correction rather than a global rewrite. The low-frequency band carries stronger cross-view agreement and larger energy, the high-frequency band is less aligned but still informative, and the low-high cosine is near zero. BRIDGE therefore uses the low bands as shared structure and the high bands as local variation, rather than treating the full representation as a single fused signal.

6.4 Additional Controls and Sensitivity

Tables 2–4 report the controls that separate the roles of DFGE, BEN, and CRI. All controls use the same splits, features, and full-sort protocol. The control suite answers three questions. First, do BEN and CRI need behavior evidence and candidate restriction, or can a generic residual work? Second, does DFGE need a spectral decomposition, or is equal-capacity routing enough? Third, does the residual mainly move score mass away from popular items, or does it improve ranking across strata? Tables 2–4 provide the quantitative controls.

Table 2 is the mechanism test. Panel (a) removes one part of BRIDGE at a time on Baby, so the table isolates the behavior branch, the multimodal encoder, and the spectral objectives. Panel (b) compares BRIDGE against alternative residual rules on three datasets, which makes it clear whether the gain comes from the calibrated score itself or from the way that score is applied.

The first row block in Table 2(a) shows that BEN and CRI are tied together. Removing behavior evidence hurts, but keeping the same evidence and relaxing the scope is still worse than the full candidate-aware model. Global correction recovers part of the drop, yet it remains below BRIDGE because the residual then reaches items that the base encoder never authorized. The message is simple: the residual helps only when it is local.

The content block in Table 2(a) shows that the item graph carries the largest share of the multimodal gain. Removing the item graph causes a sharp drop, while removing image or text alone produces smaller losses, which means the two modalities are complementary rather than interchangeable. The spectral block then separates architecture from regularization. Disabling the IB surrogate or the frequency regularizer hurts performance, but Gram, DCT, and random bases stay close to one another. The important factor is the presence of a stable band split, not a particular basis choice.

Table 2(b) answers the residual-baseline question. Raw co-occurrence is the weakest control, EASE improves it, and the conservative coefficient closes part of the gap. BRIDGE still wins on all three datasets, with the largest margin on Electronics. That result shows that BEN is not just an item-item prior. Its normalization and candidate scope matter, especially when the interaction matrix is sparse and the residual must discriminate among many near ties.

Table 3 extends the same check across datasets and fusion rules. The cross-dataset block repeats the Baby ordering on Sports and Electronics, which means the mechanism does not depend on one particular domain density. The learned-fusion block then compares a fixed residual with learned scalar mixing, an MLP gate, and an EASE-style residual. The learned variants remain close, but none surpass the fixed BRIDGE setting. In other words, a larger fusion head does not buy more than the candidate-restricted residual already provides.

Table 4 asks whether the gain comes from favoring head items. The answer is no. BRIDGE raises Recall@20 in every popularity stratum while reducing head exposure, and the effect is strongest on Sports and Electronics, where the base model is more skewed toward popular items. The conservative coefficient variant keeps more of the original exposure pattern and usually trails the fixed residual, which confirms that the simpler calibration rule is the more effective operating point.

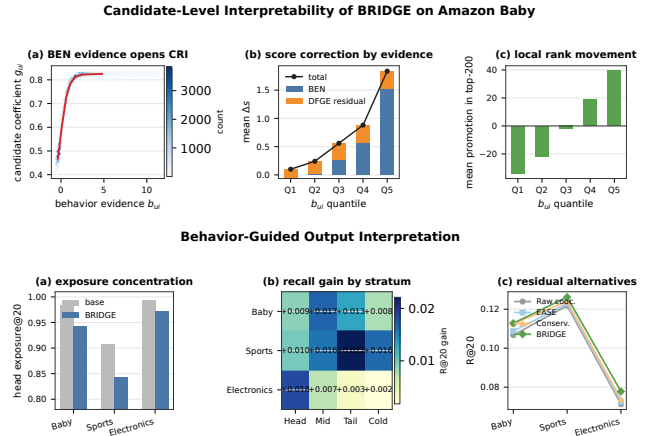


Figure 3: Compact interpretability controls for BRIDGE. BEN evidence opens CRI and produces local corrections; BRIDGE also shifts exposure while improving mid, tail, and cold recall.

The control results point to the same conclusion from different angles. Removing behavior evidence or candidate restriction consistently hurts, and global correction is weaker than candidate-level calibration. Raw co-occurrence and EASE are useful but do not match BRIDGE’s normalized residual, which shows that BEN is doing more than an ItemKNN-style lookup. On the representation side, the item graph and multimodal content are necessary, while the spectral objectives and decomposition choices mainly shape candidate geometry and stabilize the final calibrated score. Table 4 shows the same effect from the output side: BRIDGE raises mid, tail, and cold recall while lowering head exposure, so the residual redistributes ranking mass instead of amplifying popularity.

7 Discussion

The results support a frequency-first design. DFGE is not a cosmetic front end: it defines the candidate geometry on which ranking acts, and the frequency objectives keep low-frequency shared evidence and higher-frequency private variation from collapsing into one signal. BEN turns co-user overlap into signed behavior evidence, and CRI decides where that evidence may alter the score. The behavior-only, raw co-occurrence, and EASE controls show that neighborhood evidence does not replace representation learning or reduce to a generic ItemKNN signal. The learned fusion variants stay close to the fixed residual but do not exceed it, so additional calibration capacity is not the main driver. Together, the controls indicate that candidate restriction is the main safeguard against global score distortion.

Recent dual-graph, retrieval-enhanced, and dual-path alignment models point in a nearby direction: they strengthen modality interaction with extra routing, completion, or alignment modules [1, 2, 7–9, 11, 29]. BRIDGE keeps the backbone interpretable and pushes complexity into the evidence-selection rule: the base score carries the multimodal representation, and the behavior residual only decides where that score may be locally corrected.

Table 2: Core Baby ablations and cross-dataset residual alternatives. All rows use the same splits, BEIT3 features, candidate restriction, and full-sort evaluation protocol.

<i>(a) DFGE, BEN/CRI, and frequency ablations on Amazon Baby</i>					
Module	Variant	R@10	R@20	N@10	N@20
Full	BRIDGE	0.0752	0.1128	0.0428	0.0525
BEN/CRI	w/o behavior evidence	0.0682	0.1016	0.0368	0.0453
BEN/CRI	w/o top- K calibration	0.0651	0.1025	0.0354	0.0450
BEN/CRI	global correction	0.0745	0.1092	0.0419	0.0507
DFGE-Content	w/o item graph	0.0535	0.0824	0.0282	0.0356
DFGE-Content	w/o image feature	0.0735	0.1089	0.0415	0.0506
DFGE-Content	w/o text feature	0.0750	0.1089	0.0422	0.0509
DFGE-Content	w/o content features	0.0608	0.0894	0.0340	0.0414
DFGE-Spectral	w/o IB surrogate	0.0709	0.1031	0.0404	0.0487
DFGE-Spectral	w/o freq. structural reg.	0.0747	0.1107	0.0424	0.0517
DFGE-Spectral	w/o both freq. objectives	0.0712	0.1023	0.0407	0.0487
DFGE-Spectral	w/o freq. decomp. (equal cap.)	0.0746	0.1110	0.0425	0.0519
DFGE-Spectral	Gram decomposition	0.0752	0.1117	0.0425	0.0519
DFGE-Spectral	DCT decomposition	0.0751	0.1089	0.0427	0.0514
DFGE-Spectral	Random orthogonal decomp.	0.0750	0.1113	0.0427	0.0519
<i>(b) Candidate-level alternative residual controls</i>					
Dataset	Metric	Raw cooc.	EASE	Conserv. coeff.	BRIDGE
Baby	R@20	0.1067	0.1087	0.1126	0.1128
	N@20	0.0478	0.0494	0.0519	0.0525
Sports	R@20	0.1218	0.1229	0.1240	0.1262
	N@20	0.0553	0.0571	0.0589	0.0594
Electronics	R@20	0.0713	0.0724	0.0738	0.0778
	N@20	0.0338	0.0344	0.0351	0.0385

Table 3: Candidate-side controls on Amazon Baby, Sports, and Electronics. To keep the control study in the main text, we report the primary Recall@20 and NDCG@20 metrics.

<i>(a) Cross-dataset ablations</i>				<i>(b) Learned fusion controls</i>				
Dataset	Variant	R@20	N@20	Dataset	Variant	R@20	N@20	
Sports	BRIDGE	0.1262	0.0594	Baby	base encoder	0.1017	0.0455	
	conserv. coeff.	0.1217	0.0572		fixed λ mix	0.1128	0.0520	
	w/o behavior evidence	0.1162	0.0515		learned $\lambda_{\mathcal{U}}$	0.1126	0.0519	
	w/o top- K calibration	0.1127	0.0493		MLP gate	0.1115	0.0512	
	global correction	0.1137	0.0542		EASE residual	0.1087	0.0494	
	w/o calib. coeff.	0.1194	0.0567		BRIDGE	0.1128	0.0525	
	w/o behavior coeff.	0.1236	0.0581		Sports	base encoder	0.1141	0.0502
	w/o image feature	0.1208	0.0567			BRIDGE	0.1262	0.0594
	w/o text feature	0.1213	0.0572			learned $\lambda_{\mathcal{U}}$	0.1260	0.0595
	w/o content features	0.1048	0.0505			MLP gate	0.1257	0.0581
	w/o item graph	0.1010	0.0471			conserv. coeff.	0.1240	0.0589
BRIDGE	0.0778	0.0385						
Electronics	conserv. coeff.	0.0747	0.0354					
	w/o calib. coeff.	0.0755	0.0359					
	w/o behavior evidence	0.0656	0.0298					
	w/o top- K calibration	0.0647	0.0292					
	global correction	0.0642	0.0303					
	w/o image feature	0.0648	0.0293					

Table 4: Popularity-stratified diagnostic and exposure track. Head, Mid, Tail, and Cold report Recall@20 within each item-popularity stratum; Head Exp. is the top-20 exposure share assigned to head items.

Dataset	Variant	R@20	Head	Mid	Tail	Cold	Head Exp.
Baby	base	0.1017	0.1649	0.0094	0.0059	0.0031	0.9842
	mix	0.1110	0.1705	0.0270	0.0183	0.0109	0.9356
	logic	0.1113	0.1710	0.0270	0.0189	0.0109	0.9358
	BRIDGE (fixed λ)	0.1128	0.1739	0.0261	0.0189	0.0109	0.9426
Sports	base	0.1141	0.1888	0.0338	0.0217	0.0119	0.9073
	BRIDGE (fixed λ)	0.1262	0.1986	0.0497	0.0438	0.0283	0.8429
	conservative coeff. variant	0.1240	0.1926	0.0452	0.0381	0.0231	0.8658
Electronics	base	0.0637	0.0933	0.0027	0.0012	0.0006	0.9939
	BRIDGE (fixed λ)	0.0778	0.1115	0.0099	0.0045	0.0024	0.9726
	conservative coeff. variant	0.0738	0.1067	0.0067	0.0029	0.0016	0.9858

7.1 Practical Implications

A useful reading of the control suite is to separate backbone quality from residual authority. DFGE builds the candidate manifold. BEN

converts co-user overlap into signed evidence. CRI decides where that evidence may alter the score. The gain from BRIDGE comes from keeping those roles separate. When the same evidence is

allowed to act globally, it starts competing with the multimodal backbone and the improvement shrinks. Candidate restriction is therefore not an implementation detail; it is the mechanism that keeps the residual aligned with ranking.

This also explains the popularity diagnostics. Head items dominate the base ranking because they are easier to reconstruct from sparse co-occurrence, while mid, tail, and cold items depend more on cross-modal structure. BRIDGE does not impose an explicit anti-popularity penalty. It preserves head accuracy and reallocates useful mass to less exposed items that survive the candidate gate. The exposure shift in Table 4 is a by-product of better localization, not a separate regularizer.

At inference, BRIDGE adds a small residual pass over a cached candidate list. The item graph is precomputed, the behavior graph is derived from training interactions only, and the residual is never asked to rewrite the full catalog. That keeps the method compatible with standard retrieval-and-rank pipelines. The main failure mode is equally clear: if the backbone fails to place a relevant item in the candidate set, the residual cannot recover it. No calibration rule removes that ceiling.

Noisy co-user neighborhoods can also blur BEN, especially when user overlap is sparse or interaction bursts are highly local. In those settings the conservative coefficient variant is a safer operating point because it limits the magnitude of correction. The fixed candidate-weighted residual is stronger when the backbone already produces a reasonable shortlist, which is the regime targeted by the benchmark.

7.2 Calibration Behavior

The validation sweep shows that BRIDGE is not sensitive to a single hand-picked coefficient. The fixed- λ_b setting wins on all three datasets, but the conservative coefficient control remains close enough to preserve the same qualitative behavior. That matters because the residual is not trying to learn a second ranking model; it only has to decide how much local correction is safe. When the coefficient is too small, the behavior branch becomes decorative. When it is too large, it starts to fight the backbone. The five-point grid identifies the middle ground without introducing a heavy search cost.

The same pattern appears across the frequency design. The low-frequency component carries the stable cross-view structure, while the higher-frequency bands capture sparse and item-specific variation. The IB surrogate and the frequency regularizer are both needed because they serve different roles: one controls how much each node can route into the bands, the other preserves a useful band geometry once the routing has happened. The ablations show that dropping either term weakens the ranking signal, while changing the basis has only a small effect. The decomposition is therefore structural, not basis-specific.

The resulting scope is narrow on purpose. BRIDGE assumes that the base backbone already places a relevant item in the candidate set. It does not attempt to rescue items that never surface in retrieval, and it does not attempt to override a weak multimodal representation. Those limits are acceptable in the benchmark setting, where the objective is to sharpen the top of the list rather than

to replace retrieval. The design therefore fits the standard two-stage pipeline used in practical recommenders.

Because the same setup is used across all methods, the residual effect can be interpreted directly. If a baseline is strong in Recall but weak in NDCG, the calibration branch is improving ordering rather than just retrieving more items. If head exposure drops while mid and tail recall rise, the residual is redistributing ranking mass without collapsing popular items. Those are the behaviors reported by the tables and controls, so the narrative stays tied to measured outputs.

7.3 Limitations and Reproducibility

BRIDGE makes one explicit tradeoff: it keeps the base encoder as the ranking backbone and uses behavior evidence only as a local calibration signal. That choice preserves interpretability and blocks global score rewrites, but it also makes candidate quality the main ceiling on performance. If the base top- K list is weak, the residual branch cannot recover items that never enter the candidate scope. The SVD band routing adds one decomposition over each 64-dimensional channel block, yet the cost is bounded and the multimodal item graph is cached, so the additional overhead remains modest.

The implementation is reproducible from the information in this paper and the accompanying anonymous code package. The behavior graph is built only from the training split, the same BEIT3 feature files are used across all methods, and validation selects the residual weight before test evaluation. The released code stores the complete configuration, including candidate size, behavior top- K , band count, and random seed, so the reported numbers can be regenerated without any author-identifying information. The package also records the split manifest, feature paths, preprocessing scripts, and full evaluation commands, so the same results can be reproduced from the raw benchmark files without manual intervention. Because the same feature cache is used for every method, the comparison isolates ranking behavior rather than feature engineering. The reported tables use full-sort evaluation with fixed seeds and a validation-only sweep over the residual coefficient.

8 Conclusion

We presented BRIDGE, a behavior-guided residual integration framework for multimodal recommendation. BRIDGE uses DFGE to organize multimodal evidence into frequency bands, BEN to convert training-only co-user overlap into signed behavior evidence, and CRI to apply that evidence only inside the candidate set produced by the backbone. Across Baby, Sports, and Electronics, this candidate-level design improves both Recall and NDCG, with the strongest gains in NDCG, which means the method sharpens the ordering near the top of the list rather than only recovering more items at larger cutoffs.

The main lesson is that multimodal recommenders do not need a global residual rewrite to benefit from behavior evidence. They need a bounded calibration rule that acts only where the backbone has already produced plausible candidates. That separation keeps the method interpretable, reproducible, and compatible with standard two-stage pipelines. The remaining limit is explicit: if a relevant item never enters the candidate set, no residual can recover

it. Within that scope, BRIDGE provides a compact and effective operating point for top- K multimodal ranking.

References

- [1] Ji Dai, Quan Fang, Jun Hu, Desheng Cai, Yang Yang, and Can Zhao. 2026. Cross-Modal Attention Network with Dual Graph Learning in Multimodal Recommendation. *arXiv preprint arXiv:2601.11151* (2026).
- [2] Ziyuan Guo, Jie Guo, Zhenghao Chen, Bin Song, and Fei Richard Yu. 2025. IGDMMRec: Behavior Conditioned Item Graph Diffusion for Multimodal Recommendation. *arXiv preprint arXiv:2512.19983* (2025).
- [3] Ruining He and Julian McAuley. 2016. VBPR: Visual Bayesian Personalized Ranking from Implicit Feedback. In *Proceedings of the Thirtieth AAAI Conference on Artificial Intelligence (AAAI '16)*.
- [4] Xiangnan He, Kuan Deng, Xiang Wang, Yan Li, Yongdong Zhang, and Meng Wang. 2020. LightGCN: Simplifying and Powering Graph Convolution Network for Recommendation. In *Proceedings of the 43rd International ACM SIGIR Conference on Research and Development in Information Retrieval (SIGIR '20)*. 639–648. doi:10.1145/3397271.3401063
- [5] Yangqin Jiang, Lianghao Xia, Wei Wei, Da Luo, Kangyi Lin, and Chao Huang. 2024. DiffMM: Multi-Modal Diffusion Model for Recommendation. In *Proceedings of the 32nd ACM International Conference on Multimedia (MM '24)*. 7591–7599.
- [6] Chenghao Li, Wei Zhou, Yihao Zhang, Jiahao Hu, Huayi Shen, and Junhao Wen. 2026. MSCF-Net: Multi-scale Frequency Denoising and Co-frequency Enhancement Network for Multimodal Recommendation. *Expert Systems with Applications* 285 (2026), 127702. doi:10.1016/j.eswa.2026.127702
- [7] Yuan Li, Jun Hu, Jiaxin Jiang, Bryan Hooi, and Bingsheng He. 2026. Robust Multimodal Recommendation via Graph Retrieval-Enhanced Modality Completion. *arXiv preprint arXiv:2605.00670* (2026).
- [8] Yuecheng Li, Hengwei Ju, Zeyu Song, Wei Yang, Chi Lu, Peng Jiang, and Kun Gai. 2026. RecGOAT: Graph Optimal Adaptive Transport for LLM-Enhanced Multimodal Recommendation with Dual Semantic Alignment. *arXiv preprint arXiv:2602.00682* (2026).
- [9] Yang Li, Qi'ao Zhao, Chen Lin, Jinsong Su, and Zhilin Zhang. 2024. Who To Align With: Feedback-Oriented Multi-Modal Alignment in Recommendation Systems. In *Proceedings of the 47th International ACM SIGIR Conference on Research and Development in Information Retrieval (SIGIR '24)*. 667–676.
- [10] Yifan Liu, Kangning Zhang, Xiangyuan Ren, Yanhua Huang, Jiarui Jin, Yingjie Qin, Ruilong Su, Ruiwen Xu, Yong Yu, and Weinan Zhang. 2024. AlignRec: Aligning and Training in Multimodal Recommendations (CIKM '24). Association for Computing Machinery, New York, NY, USA, 1503–1512. doi:10.1145/3627673.3679626
- [11] Zihao Liu and Wen Qu. 2025. DSGRec: Dual-path Selection Graph for Multimodal Recommendation. *PeerJ Computer Science* 11 (2025), e2779. doi:10.7717/peerj-cs.2779
- [12] Haokai Ma, Yimeng Yang, Lei Meng, Ruobing Xie, and Xiangxu Meng. 2024. Multimodal Conditioned Diffusion Model for Recommendation. In *Companion Proceedings of the ACM Web Conference 2024*. doi:10.1145/3589335.3651956
- [13] Hongjian Ma, Yan Zhang, Yahui Zhou, Bing Yang, Dunhui Yu, and Zhifei Li. 2026. Let Two Graphs Talk: Self-Supervised Dual-Graph Reconstruction for Multimodal Recommendation. *Information Fusion* 125 (2026), 103462. doi:10.1016/j.inffus.2025.103462
- [14] Julian McAuley, Christopher Targett, Qinfeng Shi, and Anton van den Hengel. 2015. Image-Based Recommendations on Styles and Substitutes. In *Proceedings of the 38th International ACM SIGIR Conference on Research and Development in Information Retrieval (SIGIR '15)*. 43–52. doi:10.1145/2766462.2767755
- [15] Feng Mo, Lin Xiao, Qiya Song, Xieping Gao, Wenzhuo Song, and Shoujin Wang. 2025. FGCM: Modality-Behavior Fusion Model Integrated with Graph Contrastive Learning for Multimodal Recommendation. *IEEE Multimedia* (2025). doi:10.1109/MMUL.2025.3542757
- [16] Rongqing Kenneth Ong and Andy W. H. Khong. 2024. Spectrum-based Modality Representation Fusion Graph Convolutional Network for Multimodal Recommendation. *arXiv preprint arXiv:2412.14978* (2024).
- [17] Lin Pan, Zhiqiang Pan, Fei Cai, and Honghui Chen. 2026. Multimodal Recommender Systems: A Survey of Representation, Modeling, and Optimization. *Information Fusion* 128 (2026), 103991. doi:10.1016/j.inffus.2025.103991
- [18] Xiangchen Pan and Wei Wei. 2026. Joint Behavior-Guided and Modality-Coherence Conditional Graph Diffusion Denoising for Multi-Modal Recommendation. *arXiv preprint arXiv:2601.22498* (2026).
- [19] Yuchao Ping, Shuqin Wang, Ziyi Yang, Bugui He, Nan Zhou, and Yongqun Dong. 2024. DDRec: Dual Denoising Multimodal Graph Recommendation. *IEEE Transactions on Computational Social Systems* (2024). doi:10.1109/TCSS.2024.3490801
- [20] Yuxin Qi, Quan Zhang, Xi Lin, Xiu Su, Jiani Zhu, Jingyu Wang, and Jianhua Li. 2025. Seeing Beyond Noise: Joint Graph Structure Evaluation and Denoising for Multimodal Recommendation. In *Proceedings of the AAAI Conference on Artificial Intelligence*, Vol. 39. 12461–12469. doi:10.1609/aaai.v39i12.33358
- [21] Xuanzhe Qin, Zhuoyue Wang, Yifeng Zhang, Qin Chen, Yuhan Huang, Peng Cheng, Lei Zhang, and Peng Wang. 2026. Beyond Feature Concatenation: Mutual Information-Driven Fusion for Multimodal Sequential Recommendation. *Knowledge-Based Systems* (2026).
- [22] Steffen Rendle, Christoph Freudenthaler, Zeno Gantner, and Lars Schmidt-Thieme. 2009. BPR: Bayesian Personalized Ranking from Implicit Feedback. In *Proceedings of the Twenty-Fifth Conference on Uncertainty in Artificial Intelligence (UAI '09)*. 452–461.
- [23] Bucher Sahyouni, Matthew Vowels, Liqun Chen, and Simon Hadfield. 2026. Sequences as Nodes for Contrastive Multimodal Graph Recommendation. *arXiv preprint arXiv:2602.07208* (2026).
- [24] Zhulin Tao, Xiaohao Liu, Yewei Xia, Xiang Wang, Lifang Yang, Xianglin Huang, and Tat-Seng Chua. 2022. Self-Supervised Learning for Multimedia Recommendation. *IEEE Transactions on Multimedia* (2022).
- [25] Qifan Wang, Yinwei Wei, Jianhua Yin, Jianlong Wu, Xueming Song, and Liqiang Nie. 2021. DualGNN: Dual Graph Neural Network for Multimedia Recommendation. *IEEE Transactions on Multimedia* 25 (2021), 1074–1084.
- [26] Yinwei Wei, Xiang Wang, Liqiang Nie, Xiangnan He, and Tat-Seng Chua. 2020. Graph-Refined Convolutional Network for Multimedia Recommendation with Implicit Feedback. In *Proceedings of the 28th ACM International Conference on Multimedia (MM '20)*. 3541–3549.
- [27] Yinwei Wei, Xiang Wang, Liqiang Nie, Xiangnan He, Richang Hong, and Tat-Seng Chua. 2019. MMGCN: Multi-modal Graph Convolution Network for Personalized Recommendation of Micro-video. In *Proceedings of the 27th ACM International Conference on Multimedia (MM '19)*. 1437–1445.
- [28] Jun Wu, Yu Zheng, Tianfeng Zhang, Shilong Jing, Jinyu Liu, Shuai Guo, and Fang Deng. 2026. D-DPDC: Diffusion-based Dual-Graph Attention with Dual-Path Feature Extraction for Multimodal Recommendation. *Journal of Intelligent Information Systems* 64, 2 (2026). doi:10.1007/s10844-025-01014-7
- [29] Yuhan Xiu and Xiangrong Tong. 2026. Dual-layer Cross-modal Alignment Recommendation Based on the Diffusion Model. *Information Fusion* 125 (2026), 103472. doi:10.1016/j.inffus.2025.103472
- [30] Jie Yang, Chenyang Gu, and Zixuan Liu. 2025. Causal Inspired Multi Modal Recommendation. *arXiv preprint arXiv:2510.12325* (2025).
- [31] Wei Yang and Qingchen Yang. 2024. Multimodal-aware Multi-intention Learning for Recommendation. In *Proceedings of the 32nd ACM International Conference on Multimedia (MM '24)*. 5663–5672.
- [32] Wei Yang, Rui Zhong, Yiqun Chen, Shixuan Li, Heng Ping, Chi Lu, and Peng Jiang. 2025. FITMM: Adaptive Frequency-Aware Multimodal Recommendation via Information-Theoretic Representation Learning. In *Proceedings of the 33rd ACM International Conference on Multimedia (MM '25)*. Association for Computing Machinery, New York, NY, USA, 1–10. doi:10.1145/3746027.3755540
- [33] Wei Yang, Rui Zhong, Yiqun Chen, Chi Lu, and Peng Jiang. 2025. Structured Spectral Reasoning for Frequency-Adaptive Multimodal Recommendation. In *Advances in Neural Information Processing Systems (NeurIPS '25)*.
- [34] Yuyang Ye, Zhi Zheng, Yishan Shen, Tianshu Wang, Hengruo Zhang, Peijun Zhu, Runlong Yu, Kai Zhang, and Hui Xiong. 2025. Harnessing Multimodal Large Language Models for Multimodal Sequential Recommendation. In *Proceedings of the AAAI Conference on Artificial Intelligence*.
- [35] Jinghao Zhang, Yanqiao Zhu, Qiang Liu, Shu Wu, Shuhui Wang, and Liang Wang. 2021. Mining Latent Structures for Multimedia Recommendation. In *Proceedings of the 29th ACM International Conference on Multimedia (MM '21)*. 3872–3880.
- [36] Shanshan Zhong, Zhongzhan Huang, Daifeng Li, Wushao Wen, Jinghui Qin, and Liang Lin. 2024. Mirror Gradient: Towards Robust Multimodal Recommender Systems via Exploring Flat Local Minima. *arXiv preprint arXiv:2402.11262* (2024).
- [37] Hongyu Zhou, Xin Zhou, Lingzi Zhang, and Zhiqi Shen. 2023. Enhancing Dyadic Relations with Homogeneous Graphs for Multimodal Recommendation. In *Proceedings of the European Conference on Artificial Intelligence (Frontiers in Artificial Intelligence and Applications)*. 3124–3129. doi:10.3233/FAIA230631
- [38] Xin Zhou and Zhiqi Shen. 2023. A Tale of Two Graphs: Freezing and Denoising Graph Structures for Multimodal Recommendation. In *Proceedings of the 31st ACM International Conference on Multimedia (MM '23)*. 935–943.
- [39] Xin Zhou, Hongyu Zhou, Yong Liu, Zhiwei Zeng, Chunyan Miao, Pengwei Wang, Yuan You, and Feijun Jiang. 2023. Bootstrap Latent Representations for Multimodal Recommendation. In *Proceedings of the ACM Web Conference 2023 (WWW '23)*. 845–854.
- [40] Yan Zhou, Jie Guo, Hao Sun, Bin Song, and Fei Richard Yu. 2023. Attention-Guided Multi-Step Fusion: A Hierarchical Fusion Network for Multimodal Recommendation. In *Proceedings of the AAAI Conference on Artificial Intelligence*.
- [41] Xiaofei Zhu, Yimeng Yang, Lei Meng, Ruobing Xie, and Xiangxu Meng. 2026. Distillation Conditional Diffusion with Spectral-Enhanced Hierarchical Fusion for Multi-Behavior Recommendation. *Neurocomputing* (2026).